White Rose Research Online

eprints@whiterose.ac.uk
https://eprints.whiterose.ac.uk
Universities of Leeds, Sheffield and York

Deposited via The University of Sheffield.

White Rose Research Online URL for this paper:
https://eprints.whiterose.ac.uk/id/eprint/162876/

Version: Accepted Version

Article:
Luo, P., Madathil, S., Nishizawa, S. et al. (2020) Evaluation of dynamic avalanche performance in 1.2kV MOS-bipolar devices. IEEE Transactions on Electron Devices, 67 (9). pp. 3691-3697. ISSN: 0018-9383

https://doi.org/10.1109/TED.2020.3007594

© 2020 IEEE. Personal use of this material is permitted. Permission from IEEE must be obtained for all other users, including reprinting/ republishing this material for advertising or promotional purposes, creating new collective works for resale or redistribution to servers or lists, or reuse of any copyrighted components of this work in other works. Reproduced in accordance with the publisher's self-archiving policy.

Reuse
Items deposited in White Rose Research Online are protected by copyright, with all rights reserved unless indicated otherwise. They may be downloaded and/or printed for private study, or other acts as permitted by national copyright laws. The publisher or other rights holders may allow further reproduction and re-use of the full text version. This is indicated by the licence information on the White Rose Research Online record for the item.

Takedown
If you consider content in White Rose Research Online to be in breach of UK law, please notify us by emailing eprints@whiterose.ac.uk including the URL of the record and the reason for the withdrawal request.

UNIVERSITY OF LEEDS
University of Sheffield
UNIVERSITY of York

Evaluation of Dynamic Avalanche Performance in 1.2kV MOS-Bipolar Devices

Peng Luo, *Student Member, IEEE*, Sankara Narayanan Ekkanath Madathil, *Senior Member, IEEE*, Shin-ichi Nishizawa, *Member, IEEE*, and Wataru Saito, *Senior Member, IEEE*

***Abstract*—It is well known that Dynamic Avalanche (DA) phenomenon poses fundamental limits on the power density, turn-off power loss, dV/dt controllability and long-term reliability of MOS-bipolar devices. Therefore, overcoming this phenomenon is essential to improve energy efficiency and ensure their safe operation. In this work, detailed analysis of 1.2 kV MOS-Bipolar devices are undertaken through both calibrated TCAD simulations and experiments to show the fundamental cause of DA and the impact of current density, supply voltage as well as 3D scaling rules on the DA performance. Furthermore, the dynamic avalanche performance of a 1.2 kV NPT Trench Clustered IGBT is evaluated for high current density and low power loss operations. The results indicate that this device configuration is free of DA and can be used for ultra-high current density operation in an energy efficient manner.**

***Index Terms*—IGBT, Clustered IGBT, dynamic avalanche, dV/dt controllability, high current density operation, energy efficiency, power density.**

I. Introduction

TRENCH Insulated Gate Bipolar Transistor (TIGBT) is a key component in various power electronics applications today, such as Electric Vehicle (EV), motor drives and transportations. Recent development of TIGBTs is focused on increasing power densities and switching frequencies with the aims to compete with Wide Band Gap (WBG) power devices and achieve design optimization and cost reduction for power conversion systems [1]. Several novel technologies have been implemented to continuously improve the switching loss (E_{off}) and on-state voltage drop ($V_{ce(sat)}$) trade-off through emitter side Injection Enhancement (IE) effect [2-4]. The improvements in the E_{off}-$V_{ce(sat)}$ trade-off have resulted in not only low loss operations but also increases in current densities and improved cost performance of TIGBT modules. Low E_{off} (high dV/dt) can reduce the system size, because passive component can be shrunk with high frequency operation. However, it is found that high current density and high dV/dt during switching can induce Dynamic Avalanche (DA) within the TIGBTs, which poses fundamental limits on the power density, turn-off power loss, dV/dt controllability as well as long-term reliability of the IGBT modules [5-7]. Overcoming this phenomenon is crucial to increase energy efficiency and ensure safe operation in IGBT applications. Tremendous efforts have been devoted to suppressing DA and eliminating associated reliability concerns. Using p-layers to protect the trench bottoms can suppress but not eliminate DA in the TIGBTs [7], and the holes evacuation is not enhanced. Moreover, an asymmetric gate oxide approach with a designed variable thickness to realize stable long-term operation in TIGBTs and to reduce the switching delay and gate charge without sacrificing the electrical performance has been reported [8, 9]. However, this design cannot suppress DA and no effective designs have been proposed to eliminate DA so far.

In previous work, an in-depth analysis of the TIGBT switching behavior focusing on DA was presented through calibrated 3D TCAD models to show, for the first time, that removal of the high electric field concentration beneath the trench gates was the most important solution to manage the DA in TIGBTs. Moreover, for the first time, a DA free design with high current density operation capability was demonstrated in a Trench Clustered IGBT (TCIGBT), through in both simulations and experiments [10]. In this paper, the operation of this device is studied in detail to explain the reason for its DA free behavior. In addition, the influence of current density and supply voltage on the DA performance of TIGBTs is experimentally investigated. Finally, the impact of 3-D scaling rules of TIGBTs [3, 4] on the DA behavior is evaluated in detail.

II. Dynamic Avalanche in TIGBTs

A. Schematic of DA in TIGBTs

Fig. 1 shows the schematic of DA in the turn-off transient of trench gated IGBTs. During on-state, the carrier density ($p \approx n$) is typically in the range of 10^{16} to 10^{17} cm^{-3} due to conductivity modulation, which is at least two or three orders of magnitude higher than the background doping concentration (N_D). When the device turns off, an increase in the potential drop occurs within a small space charge region of the device with a large

Manuscript received ; revised ; accepted . The review of this article was arranged by Editor .

(Corresponding author: Peng Luo)

Peng Luo and Sankara Narayanan Ekkanath Madathil are with the Department of Electronic and Electrical Engineering, University of Sheffield, Sheffield, S1 3JD, United Kingdom (e-mail: pluo2@sheffield.ac.uk; s.madathil@sheffield.ac.uk).

Shin-ichi Nishizawa and Wataru Saito are with the Research Institute for Applied Mechanics, Kyushu University, Fukuoka 816-8580, Japan (e-mail: s.nishizawa@riam.kyushu-u.ac.jp; wataru3.saito@riam.kyushu-u.ac.jp)

Color versions of one or more of the figures in this article are available online at http://ieeexplore.ieee.org.

Digital Object Identifier

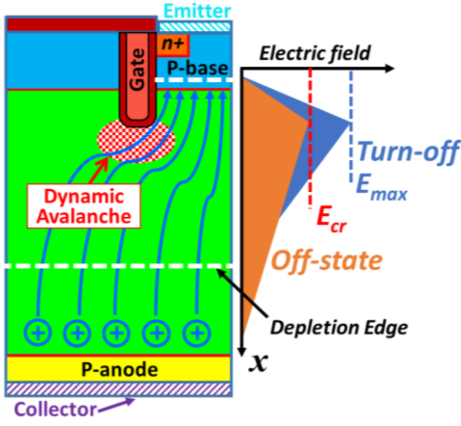

Fig. 1. Schematic of DA during turn-off of TIGBT.

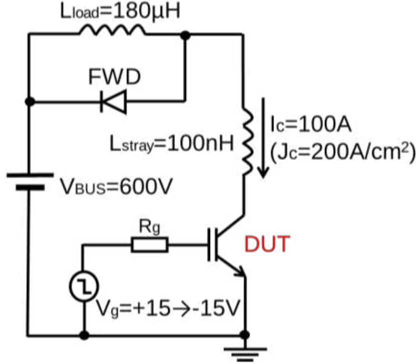

Fig. 2. Test circuit configuration.

part of stored carriers still present. The electric field distribution within the device can be expressed as

$$\frac{dE}{dx} = \frac{q}{\varepsilon}(N_D + p - n). \quad (1)$$

As depicted in Fig. 1, the stored excess holes evacuate through the P-base region, resulting in a peak electric field (E_{max}) which is much higher than the off-state electric field strength. As electric field crowds beneath trench gates, the E_{max} appears at trench bottom rather than at the P-base/N-drift junction. If the resulting E_{max} exceeds the concentration dependent critical electric field (E_{cr}), DA will be triggered even when the collector voltage is well below the off-state breakdown voltage. More excessive carriers are thus generated to result in additional E_{off} and lower dV/dt. Moreover, the excessive carriers generated due to Impact Ionization (I.I.) can have enough energy to be injected into the trench oxide to affect the gate stability and cause associated reliability concerns.

B. Influence of DA on the TIGBTs Electrical Performance

To analyze the DA in silicon TIGBTs, the 3D Sentaurus Device [11] is utilized to simulate the switching behavior, with a circuit configuration for mix-mode simulation as specified in Fig. 2. The dependence of switch-off characteristics of a 1.2 kV TIGBT in Field-Stop (FS) technology on gate resistance (R_g) is shown in Fig. 3. In practice, smaller R_g should induce larger dV/dt during turn-off, the relationship between R_g and dV/dt can be expressed as

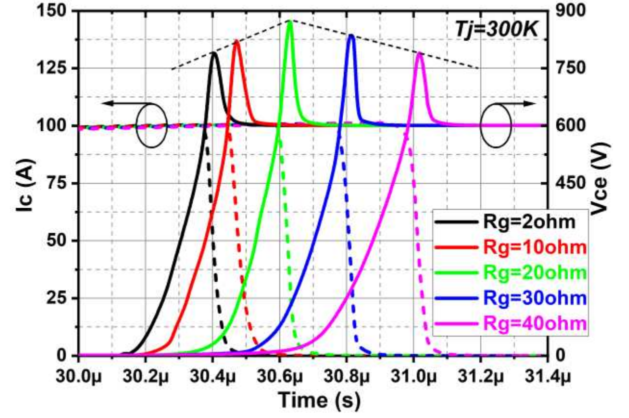

Fig. 3. Switch-off characteristics of TIGBT at various R_g.

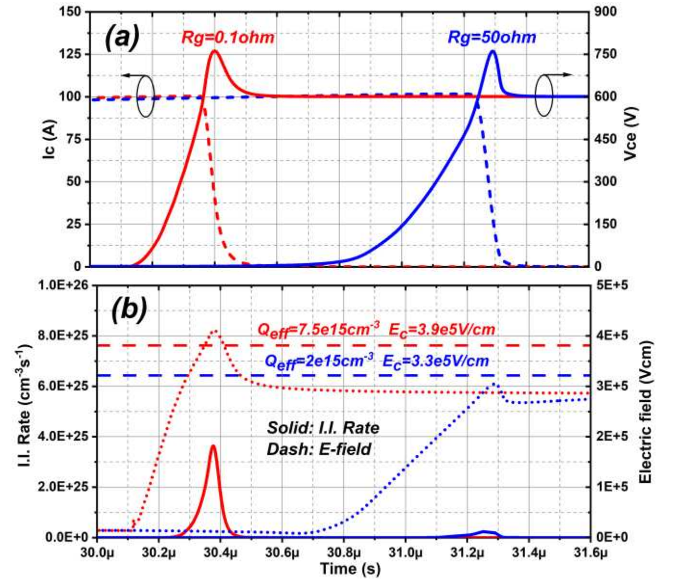

Fig. 4. Comparison of (a) Turn-off curves and (b) I.I. rates and E_{max} of a TIGBT at R_g = 0.1 Ω and R_g = 50 Ω.

$$I_g = \frac{V_{th} + I_c/g_m}{R_g} \quad (2)$$

$$\frac{dV_{CE}}{dt} = \frac{I_g}{C_{GC}} \quad (3)$$

where I_g is the gate current, V_{th} is the threshold voltage, g_m is the transconductance of the MOSFET structure, I_c is the collector current, and C_{GC} is the miller capacitance. However, the DA decreases the dV/dt, which results in decrease in surge voltage even with small R_g conditions, as shown in Fig. 3. This clearly indicates that DA occurs in the cases of R_g < 20 Ω. Fig. 4(a) compares the turn off curves while Fig. 4(b) compares the maximum electric fields (E_{max}) and maximum I.I. rates in the cases of R_g = 0.1 Ω and R_g = 50 Ω, respectively. In the case of R_g = 0.1 Ω, due to faster increase in collector voltage (higher dV/dt), the stored excessive holes do not have enough time to be evacuated from the device and flow along the trench bottom, leading to a peak electric field strength which exceeds the critical value, as shown in Fig. 4(b). The critical electric field strength is calculated with (4) and (5),

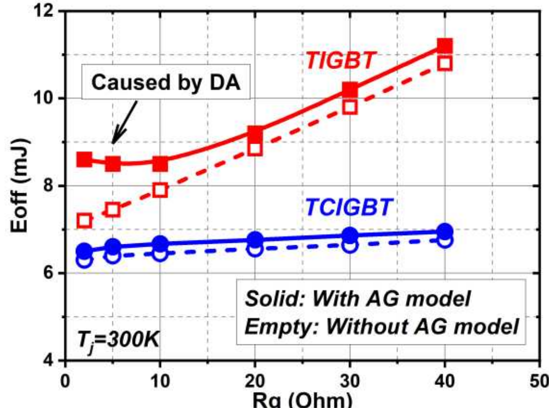

Fig. 5. Dependence of E_{off} on R_g with AG model and without AG model.

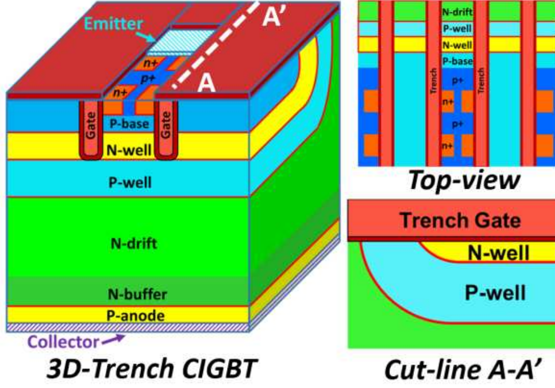

Fig. 6. 3-D cross-sectional view of TCIGBT.

$$E_{cr}(Silicon) = 4010 \times {Q_{eff}}^{1/8} \text{ [12]} \quad (4)$$

$$Q_{eff} \approx N_D + p \quad (5)$$

where Q_{eff} is the space charge at trench corner. As a result, DA occurs and generates more excessive charge to lower the dV/dt. In contrast, under large R_g conditions, the time to reach supply voltage takes longer, during which most stored charges are removed and DA does not materialize. However, this comes at the expense of increased switching loss and longer turn-off delay time. Moreover, Fig. 5 shows the simulated E_{off} with and without Avalanche Generation (AG) model. The saturation trend of E_{off} with AG model at small R_g conditions is due to DA.

In summary, DA can be triggered by high current density operation, high dV/dt condition, and current filamentation [13]. This phenomenon poses fundamental limits on operating current density, switching frequency, dV/dt controllability, and leads to reliability issues due to hot carrier effect. Therefore, eliminating DA is essential for the development of TIGBTs.

III. Dynamic Avalanche Free Design: TCIGBT

Fig. 6 shows the 3D cross-sectional view of the TCIGBT. The TCIGBT features a MOS-gated thyristor structure, which consists of P-anode, N-drift, P-well and N-well. Its turn-on mechanism has been explained in [14]. In the on-state, the N-well and P-well are conductivity modulated and the device undergoes self-clamping. During turn-off, due to self-clamping,

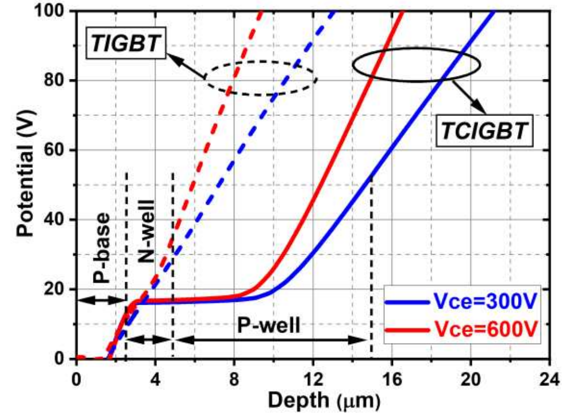

Fig. 7. Simulated potential distributions as a function of collector voltage during turn-off of the TIGBT and TCIGBT.

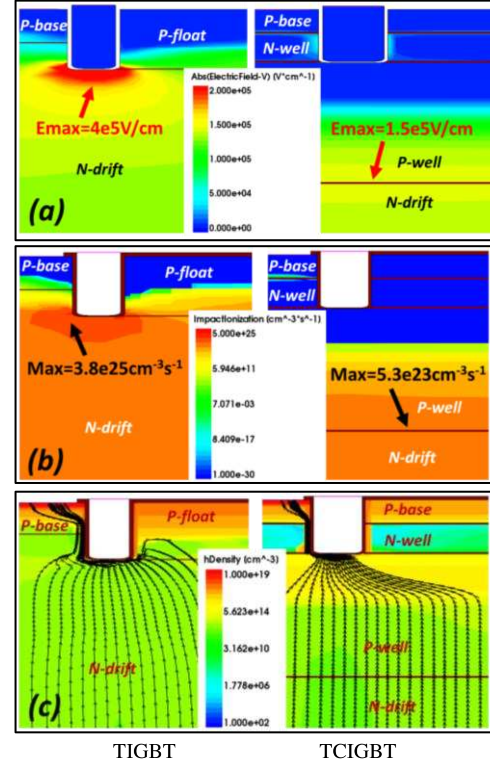

Fig. 8. Comparison of (a) electric field distributions, (b) I.I. rate distributions and (c) hole densities when V_{ce} raises to 600V ($R_g = 0.1\ \Omega$).

the potential of the N-well layer, which acts as the body of the PMOS is held at a fixed collector potential of less than 20 V, which is the self-clamping voltage of the TCIGBT, as shown in Fig. 7. When the gate voltage decreases below its threshold voltage, because of the increase in body potential, holes are formed along the sidewall of trench gates to connect the P-well layer with P-base region through PMOS action, as shown in Fig. 8(c). Therefore, whether the gate potential goes negative or not during turn-off has no impact on the turn-off behavior. Such a unique design, not available in TIGBTs, provides a direct evacuation path for excess holes to be collected within emitter region. The E_{off} is thus significantly reduced compared to the TIGBT, as shown in Fig. 5. Moreover, as the collector voltage is supported by the P-well/n-drift junction, the trench gates are protected from high electric field so that there is no electric field

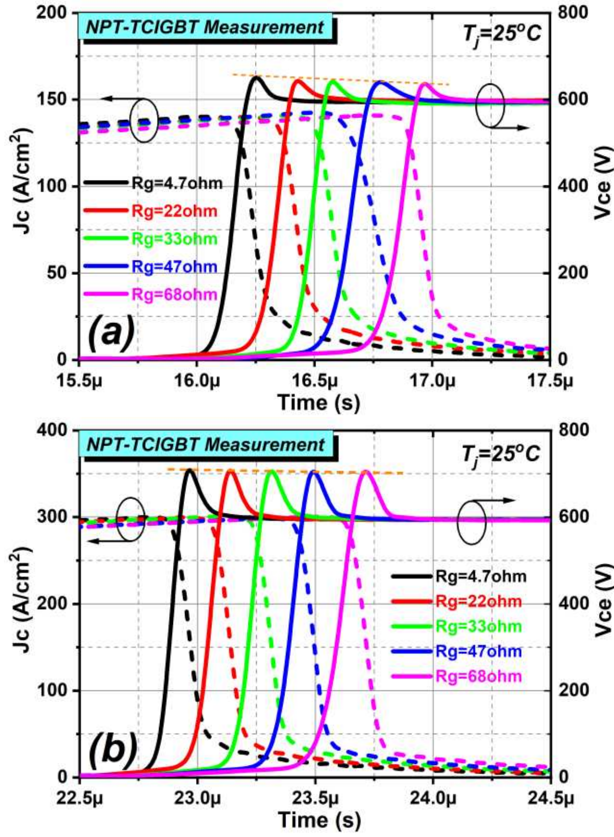

Fig. 9. Experimental switch-off curves of TCIGBT at various R_g at (a) J_c = 140 A/cm² and (b) J_c = 300 A/cm².

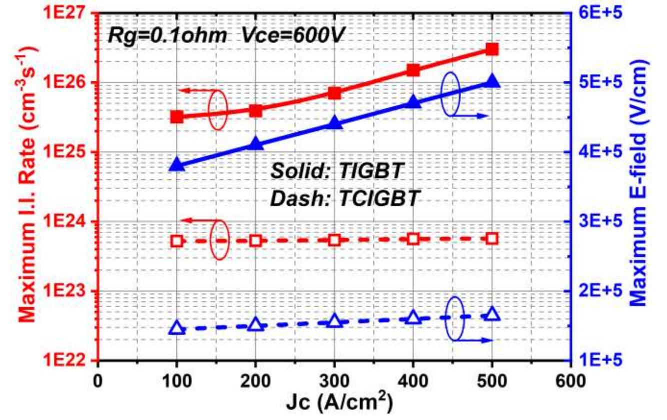

Fig. 10. Impact of current density on E-field and I.I. rate during turn-off.

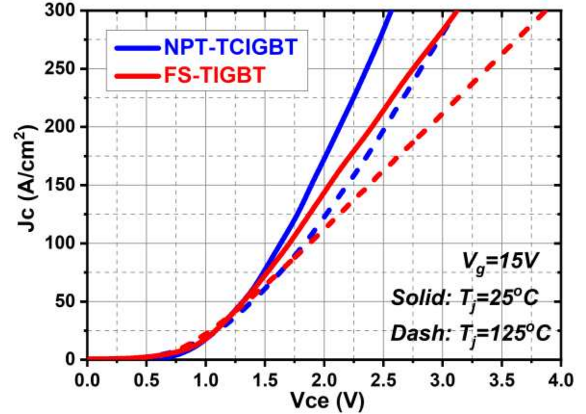

Fig. 11. Experimental results of the I-V curves of TIGBT and TCIGBT.

crowding in TCIGBT, as shown in Fig. 8(a). Thus, it provides a fundamental solution for electric field management at trench regions to prevent occurrence of DA, as shown in Fig. 5.

Figs. 8(a), (b) and (c) show a comparison of the electric field distributions, I.I. rates and hole densities at the time point of V_{ce} increases to 600 V between TIGBT and TCIGBT under R_g = 0.1 Ω and identical $V_{ce(sat)}$ conditions, respectively. As can be seen, the trench gates of TCIGBT are protected from high electric field concentrations during turn-off. In comparison, the TIGBT shows a strong electric field crowding in excess of the E_{cr} under the trench bottom and leads to a high I.I. rate.

Absence of DA in TCIGBT is clear from the experimental results of the switching waveforms of 1.2 kV TCIGBTs measured as a function of R_g, as shown in Figs. 9(a) and (b). These devices show a $V_{ce(sat)}$ of 1.8 V at 140 A/cm² at Room Temperature (R.T.) and can support 1.6 kV and are short circuit proof [15]. Although the demonstrated devices were made in Non-Punch-Through (NPT) technology, moving to a thinner FS technology has no impact on the DA, as discussed later. Fig. 9(b) shows that TCIGBT does not show DA even at J_c = 300 A/cm². This confirms that TCIGBT can be operated at high current density without DA and associated reliability concerns and with very low power losses.

IV. Impact of Current Density on DA Performance

The continuous increase of power density is crucial for the development of IGBTs to achieve low cost and design optimization for power electronic systems. Higher power density requires higher operating current density as well as low power loss per chip area. However, Fig. 10 shows that DA is significantly enhanced at high current density operations, which poses a limit on the operating current density of TIGBTs. In order to clarify the influence of current density on the DA performance, a 1.2 kV 25 A TIGBT device in FS technology [16] was investigated in detail and compared with the measured results of a 1.2 kV NPT TCIGBT. Fig. 11 shows the comparison of the measured IV characteristics at 25 ºC and 125 ºC. Despite the fact that the FS TIGBT (device thickness = 115 µm) features a much thinner device thickness than the NPT TCIGBT (device thickness = 200 µm), the TCIGBT shows much lower on-state losses in comparison to that of TIGBT at both rated current density (J_c = 140 A/cm²) and high current densities due to thyristor conduction. The other characteristics of NPT-TCIGBT and FS-TIGBT have been reported in [15]. Fig. 12 shows the measured E_{off} of the TIGBT as a function of R_g at various operating current densities. The E_{off} increases more significantly at small R_g in the case of high current density operations due to enhanced DA. In contrast, the self-clamping feature ensures TCIGBTs to remain DA free performance at high current density operations, as shown in Fig. 13. The E_{off} shows linear decreases as R_g reduces at both R.T. and 125 ºC. Therefore, TCIGBTs are well suited for operating at high current densities without DA effects.

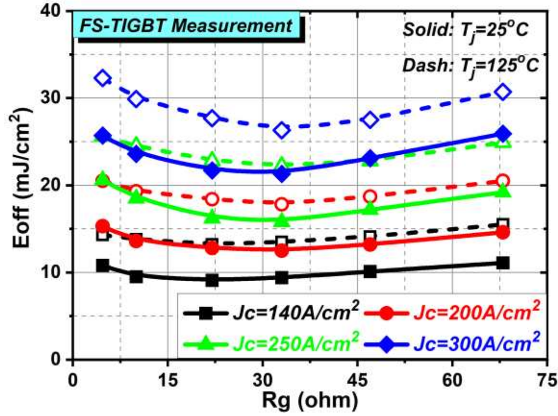

Fig. 12. Impact of current density on the E_{off} of TIGBT.

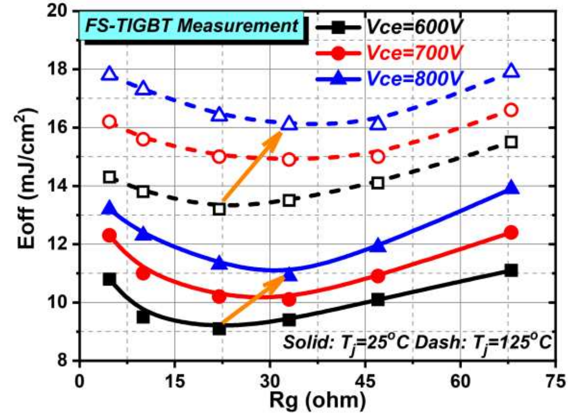

Fig. 15. Impact of supply voltage on the E_{off} of TIGBT.

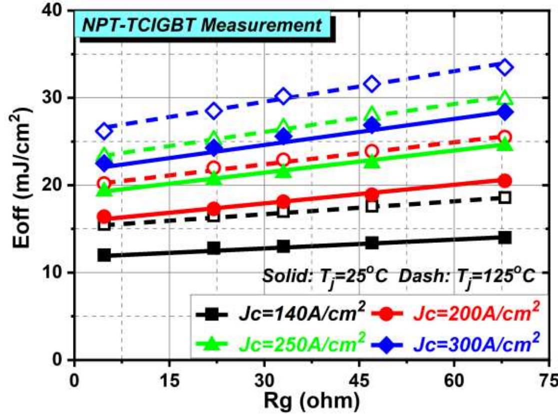

Fig. 13. Impact of current density on the E_{off} of TCIGBT.

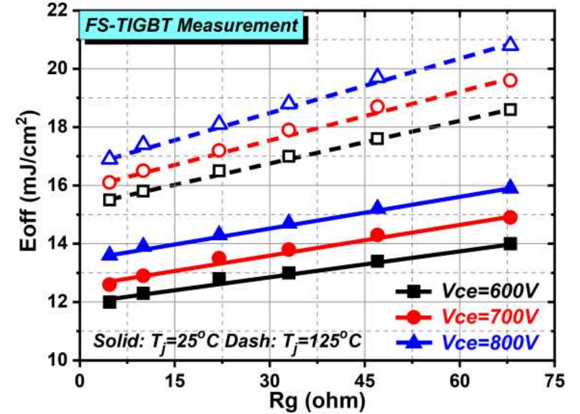

Fig. 16. Impact of supply voltage on the E_{off} of TCIGBT.

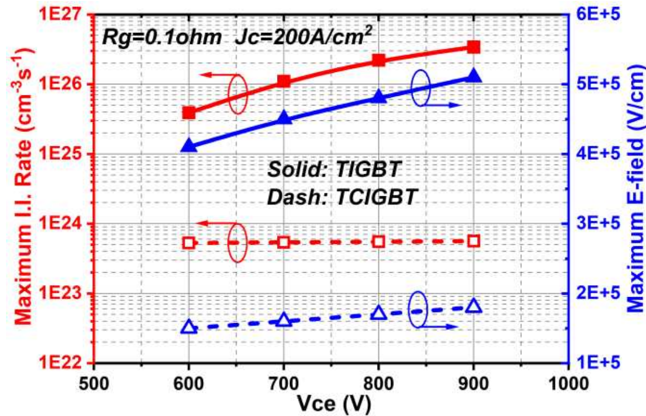

Fig. 14. Impact of supply voltage on E-field and I.I. rate during turn-off.

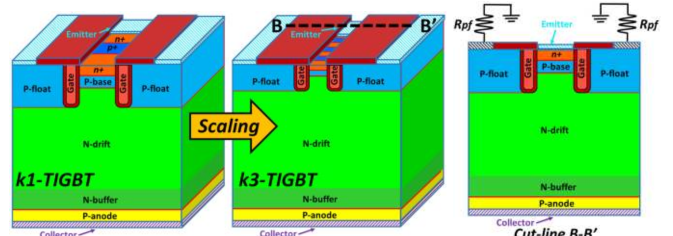

Fig. 17. 3-D scaling rules of TIGBT [4]. Structural parameters are from [4].

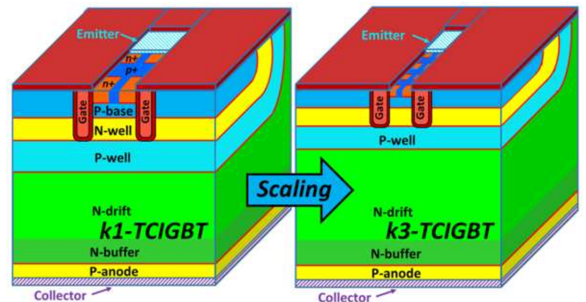

Fig. 18. 3-D scaling rules of TCIGBT. Structural parameters of cathode cells are from [17].

V. Impact of Supply Voltage on DA Performance

As the collector voltage has a direct impact on the electric field strength within the TIGBT during turn-off, the DA phenomenon is enhanced as supply voltage increases, as shown in Fig. 14. The measured E_{off} of the TIGBT as a function of R_g at various supply voltages is shown in Fig. 15. Note that the minimum E_{off} at V_{ce} = 800 V appears at a larger R_g in comparison to the case of V_{ce} = 600 V, which confirms that higher supply voltage enhances the DA performance of TIGBTs. In contrast, the supply voltage has no impact on the DA free performance of TCIGBT, as shown in Fig. 16.

VI. Impact of 3D Scaling Rules on DA Performance

To understand the impact of the 3D scaling rules on the DA performance of the devices, scaled TIGBTs [4] as well as scaled TCIGBTs [17] in FS technologies are considered, as shown in

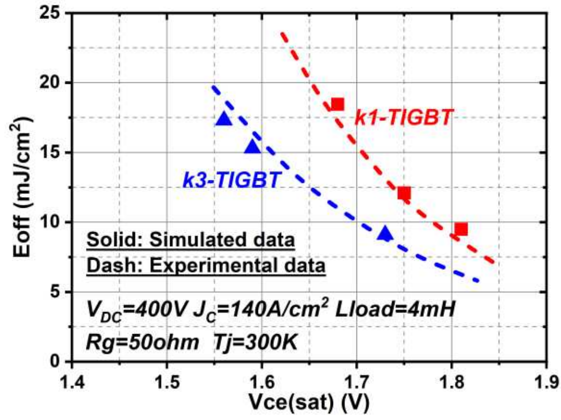

Fig. 19. Calibration of simulated 3-D TIGBT models with experimental data in [4].

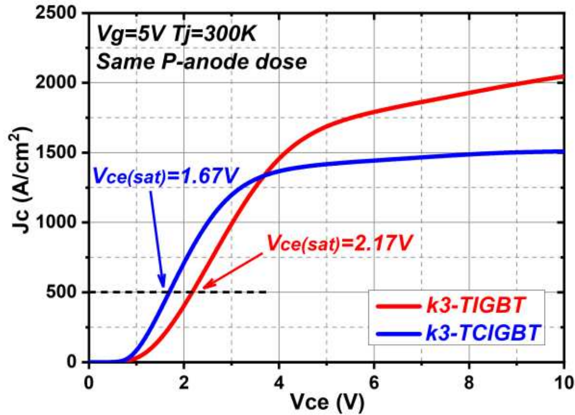

Fig. 20. Comparison of *I-V* curves between *k3*-TIGBT and *k3*-TCIGBT.

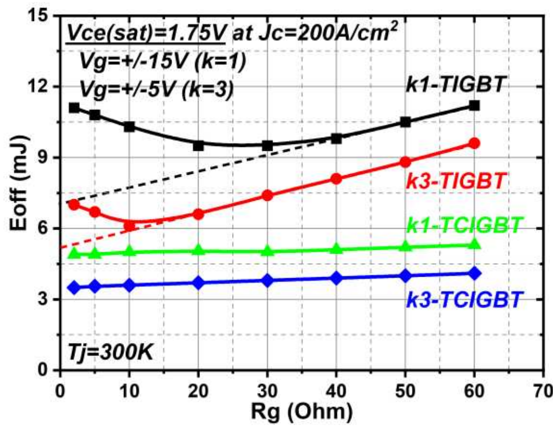

Fig. 21. Impact of E_{off} versus R_g with scaling in TIGBTs and TCIGBTs under same $V_{ce(sat)}$ condition.

Fig. 17 and Fig. 18, respectively. The structures were evaluated through 3D modelling with models calibrated against measured data, as shown in Fig. 19. Note that the device thickness in all structures are identical as in [4] in order to compare the electrical characteristics. Fig. 20 compares the *I-V* curves of *k3*-TIGBT and *k3*-TCIGBT under identical threshold voltage and same P-anode conditions. The *k3*-TCIGBT yields a low $V_{ce(sat)}$ of 1.67 V even at J_c = 500 A/cm^2 at R.T., which is 23 % lower than that of *k3*-TIGBT. Furthermore, the non-saturated *I-V* behavior of narrow mesa TIGBTs is effectively suppressed in

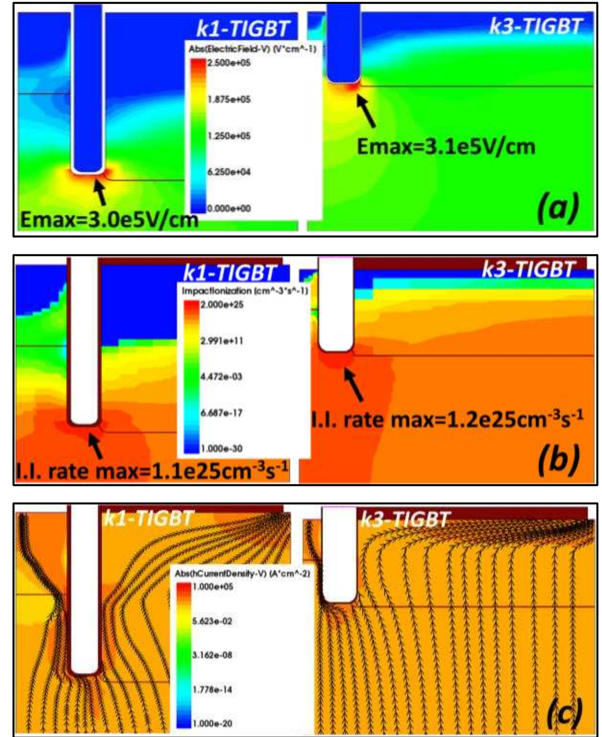

Fig. 22. Comparison of (a) electric field distributions, (b) I.I. rates and (c) hole densities when V_{ce} raises to 600 V (R_g = 20 Ω).

k3-TCIGBT due to enhanced self-clamping feature [17]. The E_{off} dependence on R_g between scaled TIGBTs and TCIGBTs were compared under same $V_{ce(sat)}$ conditions, as shown in Fig. 21, which is achieved by adjusting P-anode concentration. The low switching losses of both devices decrease as a function of scaling rule. Moreover, the lower losses of *k3*-TCIGBT is clear as shown in Fig. 21. In TIGBT, 3D-scaling rule does not suppress DA, because enhanced IE effect influences are stronger than relaxation of electric field concentration as shown in Fig. 22. However, as can be observed from Fig. 21, *k3*-TIGBT does not show any obvious increase in E_{off}, which is due to fast hole evacuation by shallow trench. In any case, care must be taken to address reliability concerns with thinner gate oxides in TIGBTs.

The impact of the on-state carrier profile on DA in *k3*-TIGBT is analyzed by changing the resistance R_{pf} between the p-float region and the emitter, as shown in Fig. 23(a). The carrier concentration at the emitter-side can be increased with high R_{pf} due to the IE effect. The rate of change of voltage (dV/dt) is increased with decrease in R_{pf} (Fig. 23(b)). Both I.I. rates and E_{max} values are enhanced by the positive charge of excess holes around the trench gate bottom (Fig. 23(c)). Most importantly, these results shown in Fig. 23 demonstrate that diversion of holes away from the trench bottom alone does not suppress DA. In Figs. 24(a), (b) and (c) are shown some analysis of DA due to the increase in carrier concentration at the collector-side. Although the turn-off time can be increased by increasing P-anode concentration (Fig. 24(b)), the collector-side carrier concentration has no influence on the DA performance of *k3*-TIGBT (Fig. 24(c)).

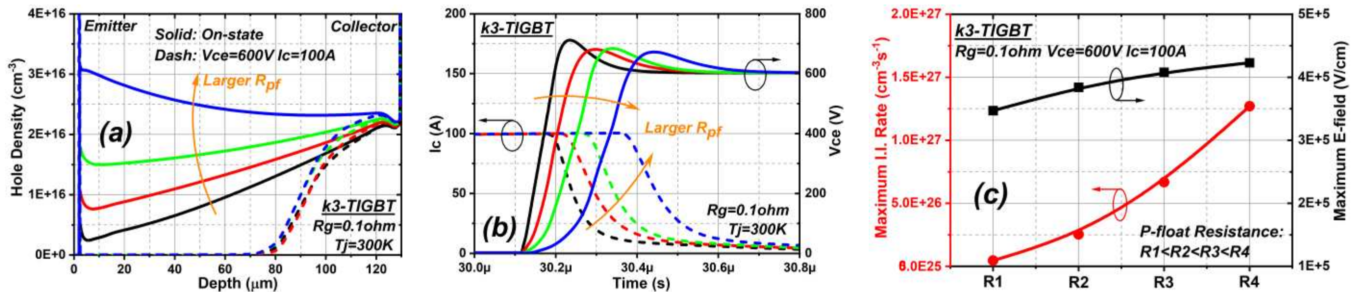

Fig. 23. Influence of R_{pf} on (a) on-state hole density and excess hole density when V_{ce} raises to 600 V, (b) switch-off characteristics, and (c) maximum electric field and maximum I.I. rate when V_{ce} raises to 600 V in the case of *k3*-TIGBT. (V_g = +/- 5 V)

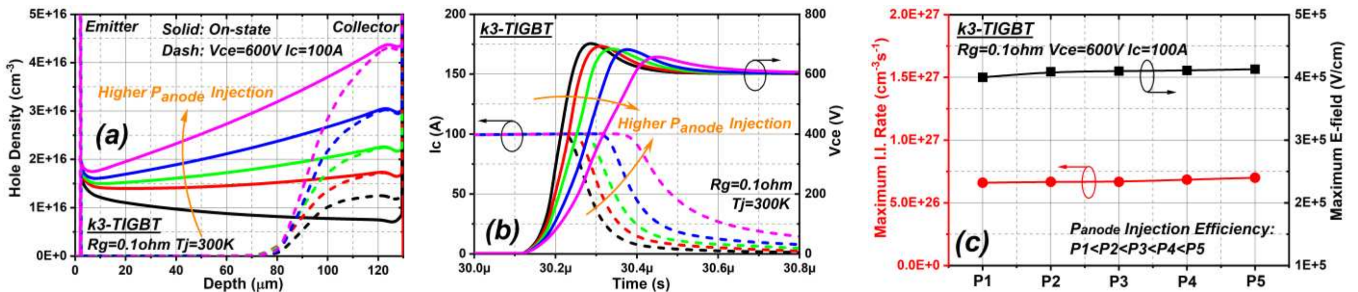

Fig. 24. Influence of anode injection efficiency on (a) on-state hole density and excess hole density when V_{ce} raises to 600 V, (b) switch-off characteristics, and (c) maximum electric field and maximum I.I. rate when V_{ce} raises to 600 V in the case of *k3*-TIGBT. (V_g = +/-5 V)

VII. Conclusions

The 1.2 kV Trench IGBT (TIGBT) switching behavior focusing on the DA was analyzed through calibrated 3D TCAD models. Management of the electric field concentration beneath trench gates is the most critical way to minimize the DA. In addition, a DA free turn-off operation is demonstrated in a Trench Clustered IGBT (TCIGBT), through in both simulations and experiments. As a MOS controlled thyristor device, TCIGBT can be operated with very low power losses at high current densities without DA and associated reliability concerns. This is because of the its PMOS action, which eliminates electric field crowding at trench bottom during turn-off transients. Moreover, experimental results confirm that DA is enhanced at high current densities and high supply voltages and results in significant increase in E_{off} in the TIGBTs. In comparison, TCIGBTs remain DA free performance at high current density operations and high supply voltage conditions. Low turn-off energy loss can be easily achieved by reducing gate resistance. Finally, the impact of device scaling design on the DA has also been analyzed with calibrated models.

References

[1] T. Laska, "Progress in Si IGBT Technology – as an ongoing Competition with WBG Power Devices," in *IEDM Tech. Dig.*, Dec. 2019, pp. 12.2.1-12.2.4, doi: 10.1109/IEDM19573.2019.8993459.

[2] C. Jaeger, A. Philippou, A. V. Ilei, J. G. Laven, and A. Härtl, "A new sub-micron trench cell concept in ultrathin wafer technology for next generation 1200 V IGBTs," in *Proc. 29th Int. Symp. Power Semiconductor Devices and IC's (ISPSD)*, May 2017, pp. 69-72, doi: 10.23919/ISPSD.2017.7988895.

[3] K. Kakushima, T. Hoshii, K. Tsutsui, A. Nakajima, S. Nishizawa, H. Wakabayashi, I. Muneta, K. Sato, T. Matsudai, W. Saito, T. Saraya, K. Itou, M. Fukui, S. Suzuki, M. Kobayashi, T. Takakura, T. Hiramoto, A. Ogura, Y. Numasawa, I. Omura, H. Ohashi, and H. Iwai, "Experimental verification of a 3D scaling principle for low $V_{ce(sat)}$ IGBT," in *IEDM Tech. Dig.*, Dec. 2016, pp..6.1-10.6.4, doi: 10.1109/IEDM.2016.7838390.

[4] T. Saraya, K. Itou, T. Takakura, M. Fukui, S. Suzuki, K. Takeuchi, M. Tsukuda, Y. Numasawa, K. Satoh, T. Matsudai, W. Saito, K. Kakushima, T. Hoshii, K. Furukawa, M. Watanabe, N. Shigyo, K. Tsutsui, H. Iwai, A. Ogura, S. Nishizawa, I. Omura, H. Ohashi, and T. Hiramoto, "Demonstration of 1200V Scaled IGBTs Driven by 5V Gate Voltage with Superiorly Low Switching Loss," in *IEDM Tech. Dig.*, Dec. 2018, pp. 8.4.1-8.4.4, doi: 10.1109/IEDM.2018.8614491.

[5] T. Ogura, H. Ninomiya, K. Sugiyama, and T. Inoue, "Turn-off switching analysis considering dynamic avalanche effect for low turn-off loss high-voltage IGBTs," *IEEE Trans. Electron Devices,* vol. 51, no. 4, pp. 629-635, Apr. 2004, doi: 10.1109/TED.2004.825109.

[6] J. Lutz and R. Baburske, "Dynamic avalanche in bipolar power devices," *Microelectronics Reliability,* vol. 52, no. 3, pp. 475-481, Mar. 2012, doi: 10.1016/j.microrel.2011.10.018.

[7] S. Machida, K. Ito, and Y. Yamashita, "Approaching the limit of switching loss reduction in Si-IGBTs," in *Proc. 26th Int. Symp. Power Semiconductor Devices and IC's (ISPSD)*, Jun. 2014, pp. 107-110, doi: 10.1109/ISPSD.2014.6855987.

[8] C. Sandow, P. Brandt, H. Felsl, F. Niedernostheide, F. Pfirsch, H. Schulze, A. Stegner, F. Umbach, F. Santos, and W. Wagner, "IGBT with superior long-term switching behavior by asymmetric trench oxide," in *Proc. 30th Int. Symp. Power Semiconductor Devices and IC's (ISPSD)*, May 2018, pp. 24-27, doi: 10.1109/ISPSD.2018.8393593.

[9] L. Ngwendson, I. Deviny, C. Zhu, I. Saddiqui, J. Hutchings, C. Kong, Y. Wang, and H. Luo, "New Locos Trench Oxide IGBT Enables 25% Higher Current Density in 4.5kV/1500A Module," in *Proc. 31th Int. Symp. Power Semiconductor Devices and IC's (ISPSD)*, May 2019, pp. 323-326, doi: 10.1109/ISPSD.2019.8757651.

[10] P. Luo, E. M. S. Narayanan, S. Nishizawa, and W. Saito, "Dynamic Avalanche Free Design in 1.2kV Si-IGBTs for Ultra High Current Density Operation," in *IEDM Tech. Dig.*, Dec. 2019, pp. 12.3.1-12.3.4, doi: 10.1109/IEDM19573.2019.8993596.

[11] I. Synopsys, *Sentaurus Device User Guide*: Ver. L-2017. 09.

[12] B. J. Baliga, *Fundamentals of power semiconductor devices*: New York, NY, USA, Springer, 2016.

[13] Y. Shiba, I. Omura, and M. Tsukuda, "IGBT avalanche current filamentaion ratio: Precise simulations on mesh and structure effect," in *Proc. 28th Int. Symp. Power Semiconductor Devices and IC's (ISPSD)*, Jun. 2016, pp. 339-342, doi: 10.1109/ISPSD.2016.7520847.

[14] O. Spulber, M. Sweet, K. Vershinin, C. K. Ngw, L. Ngwendson, J. V. S. C. Bose, M. M. D. Souza, and E. M. S. Narayanan, "A novel trench clustered insulated gate bipolar transistor (TCIGBT)," *IEEE Electron Device Lett.,* vol. 21, no. 12, pp. 613-615, Dec. 2000, doi: 10.1109/55.887483.

[15] H. Y. Long, M. R. Sweet, M. M. D. Souza, and E. M. S. Narayanan, "The next generation 1200V Trench Clustered IGBT technology with improved trade-off relationship," in *Proc. Applied Power Electronics Conference and Exposition (APEC)*, Mar. 2015, pp. 1266-1269, doi: 10.1109/APEC.2015.7104510.

[16] Datasheet: Infineon IGBT, Available: http://pdf.tixer.ru/517408.pdf [Online].

[17] P. Luo, H. Y. Long, M. R. Sweet, M. M. D. Souza, and E. M. S. Narayanan, "Numerical Analysis of 3-D Scaling Rules on a 1.2-kV Trench Clustered IGBT," *IEEE Trans. Electron Devices,* vol. 65, no. 4, pp. 1440-1446, Feb. 2018, doi: 10.1109/TED.2018.2807318.